P3-044

Deuterium trapping and release in Be(0001), Be(11-20) and polycrystalline beryllium

R. Piechoczek*[1], M. Reinelt[1], M. Oberkofler[1], A. Allouche[2], and Ch. Linsmeier[1]

[1] *Max-Planck-Institut für Plasmaphysik, EURATOM Association, Boltzmannstr. 2, D-85748 Garching b. München, Germany*
[2] *Physique des Interactions Ioniques et Moléculaires, CNRS / Université de Provence, Campus Saint Jérôme, Service 242, 13397 Marseille Cedex 20, France*

Abstract

The atomistic understanding of retention and release processes of deuterium in beryllium is reached by comparing well-defined experiments on Be(0001) and Be(11-20) single crystals, as well as polycrystalline Be to simulations. The experimental desorption spectra are modelled as a coupled reaction diffusion system (CRDS). The single atomistic steps are described by a set of rate equations. Activation energies for the single processes are calculated from density functional theory. At D fluences of ~3×10^{19} m^{-2} one single D release peak around 750 K is observed. Peak shifts on the order of 10 K are observed for different implantation depths and crystal orientations. D retention in Be(11-20) is close to 100%, whereas in Be(0001) only ~60% are retained. The reduced retention in Be(0001) is attributed to anisotropic self-interstitial diffusion influencing the availability of monovacancy traps during implantation. Additionally, desorption spectra with various temperature ramps recorded on polycrystalline Be were successfully reproduced with the CRDS code. D_2 release from polycrystalline Be occurs at lower temperatures than from the single crystals. This is attributed to fast D diffusion along grain boundaries.

PACS: 28.52.Fa; 34.35.+a; 68.65.Ln; 68.63.bd

PSI-20 Keywords: Beryllium, Deuterium retention, Diffusion, Defects, First Wall

Corresponding Author:

Rainer Piechoczek
Boltzmannstr. 2
D-85748 Garching
Mail: rainer.piechoczek@ipp.mpg.de

Presenting Author :

Christian Linsmeier
Boltzmannstr. 2
D-85748 Garching
Mail: linsmeier@ipp.mpg.de

1. Introduction

Our goal is to identify the fundamental atomistic mechanisms for D retention and thermal release in Be. Well-defined implantation and release experiments yield characteristic desorption spectra which are interpreted by applying models based on coupled reaction diffusion rate equations. The respective activation energies for the atomistic reaction steps are determined in density functional theory (DFT) calculations [1]. The most critical property of beryllium is the strongly anisotropic diffusivity of self interstitials and hydrogen parallel and perpendicular to the Be basal planes, clearly demonstrated by the DFT results. We choose Be(0001) and Be(11-20) crystal orientations with surfaces parallel and perpendicular to the Be basal planes for the experiments. The ITER beryllium first wall will consist of polycrystalline beryllium, therefore we compare the experiments on single crystals to identical measurements on polycrystalline Be. By applying the singly crystal mechanisms and grain boundary effects, we are able to consistently describe the D retention and release results also for polycrystalline material.

2. Experimental

In-situ experiments are performed at the ARTOSS [2] machine at the IPP with a base pressure of $\leq 4\times10^{-11}$ mbar. Detailed information on experimental setup and procedure are published elsewhere [3]. Single and polycrystalline Be samples are cleaned by Ar+ sputtering and subsequent 1000 K annealing cycles. X-ray photoelectron spectroscopy shows less than 1 monolayer of oxygen coverage for the clean samples. D_3^+ ions are implanted at 1 and 3 keV/D with constant fluences and fluxes. Retained amounts of D in Be are attained by nuclear reaction analysis. Temperature programmed desorption spectrometry (TPD) of the

single crystals is done at 0.7 K/s heating rate (Fig. 1). The ramps in experiments with polycrystalline Be are 0.1, 0.2, 0.7 and 2.0 K/s (Fig. 3). At a low D fluence of 3×10^{19} m^{-2} only one D_2 release peak at 750 K is observed.

3. Modelling

To model these experimental results we use a description based on coupled reaction diffusion systems (CRDS [4]). The time evolution of the number density ρ [m^{-3}] of a species A is calculated by a diffusion term (Fick's second law) and reaction rate Φ [$m^{-3}s^{-1}$] that allows for an exchange of the species, thus coupling all species by local processes (equ. 1). An additional term S [$m^{-3}s^{-1}$] is used to change the density by external sources such as implantation. Because of the anisotropy of the diffusion processes, two spatial dimensions x and z are used. The diffusivity D has therefore different values depending on the spatial direction and is implemented in the general form as equ. 2 with λ [m] as the lattice constant and ν_0 [s^{-1}] as the vibrational frequency of the Be lattice.

$$\frac{\partial \rho_A(x,z,t)}{\partial t} = \frac{\partial}{\partial x}\left(D_A^x(T) \frac{\partial \rho_A(x,z,t)}{\partial x} \right) + \frac{\partial}{\partial z}\left(D_A^z(T) \frac{\partial \rho_A(x,z,t)}{\partial z} \right) + \Phi_A(x,z,t) + S_A(x,z,t) \quad [1]$$

$$D_A^{x,z} = \nu_0 \lambda_{x,z}{}^2 \exp\left(-\frac{\Delta E_{x,z}}{k_B T} \right) \quad [2]$$

Local reaction processes are given in the form of activated Arrhenius terms (equ. 3-6). In addition to the usual trapping (equ. 3) / de-trapping (equ. 4) reactions [4], the annihilation of Frenkel pairs (equ. 6) and a self-trapping term (equ. 5) are needed to reproduce the experimentally observed TPD peak forms, as was shown in [4]. The annihilation reaction uses the lowest diffusion barrier of the involved species.

$$H + MV \rightarrow HV: \qquad \Gamma_{Trapping} = \frac{\rho_{MV}}{\rho_{Be}} \rho_H \nu_0 \exp\left(\frac{-\Delta E_{Trapping}}{k_B T} \right) \quad [3]$$

$$HV \rightarrow H + MV: \qquad \Gamma_{Detrapping} = \rho_{HV} \nu_{Detrapping} \exp\left(\frac{-\Delta E_{Trapping}}{k_B T}\right) \qquad [4]$$

$$H + HV \rightarrow 2HV + SIA: \qquad \Gamma_{Selftrapping} = \rho_{HV} \nu_{Selftrapping} \exp\left(\frac{-\Delta E_{Selftrapping}}{k_B T}\right) \qquad [5]$$

$$MV + SIA \rightarrow -: \qquad \Gamma_{Anihilation} = \frac{\rho_{MV}}{\rho_{Be}} \rho_{SIA} \nu_0 \exp\left(\frac{-\Delta E_{Anihilation}}{k_B T}\right) \qquad [6]$$

For each species, those reaction fluxes are summed up which change the number density of the species, weighted by the stoichiometry factor of the respective reaction. The sign of each term is positive, if the reaction increases the density of species, or negative, if the species is consumed by the reaction (equ. 7-10). As species of the model we select hydrogen (H), Be self interstitials (SIA), monovacancies (MV) and a hydrogen-vacancy-complex (HV). In the case of the low fluences of the experiments with single crystals, this is a reasonable choice, because the implantation cascades as a first approximation produce Frenkel Pairs (SIA+MV), which are the first possible trap sites for hydrogen during the cascade. This is also in agreement with DFT calculations [1], where monovacancies are a possible trap site for hydrogen. Hydrogen H is here used synonymously for all hydrogen isotopes.

$$\Phi_H = +\Gamma_{Detrapping} - \Gamma_{Trapping} - \Gamma_{Selftrapping} \qquad [7]$$

$$\Phi_{HV} = +\Gamma_{Trapping} - \Gamma_{Detrapping} + \Gamma_{Selftrapping} \qquad [8]$$

$$\Phi_{MV} = +\Gamma_{Detrapping} - \Gamma_{Trapping} - \Gamma_{Anihilation} \qquad [9]$$

$$\Phi_{SIA} = +\Gamma_{Selftrapping} - \Gamma_{Anihilation} \qquad [10]$$

This model is implemented in Mathematica and equ. 1 is solved numerically, applying von Neumann boundary conditions at both sides in x direction. For homogeneous profiles in x direction, this is equivalent to a periodic boundary condition. The boundary condition in both z surfaces is 0 for all species. Since the surface is a perfect sink for lattice defects, this assumption is justified. Moreover, it was shown experimentally that surface processes for hydrogen are not release limiting in this temperature range. This means that hydrogen desorbs readily if the surface is reached. The resulting TPD fluxes for the upper (z_0) and lower surface (z_{max}) are calculated from equ. 11.

$$\Gamma_{TPD} = D_H^z \frac{\partial \rho((z = z_0, z_{\max}), x, t)}{\partial z} \quad [11]$$

The initial configuration is an empty sample (x_{max} = 1 nm, z_{max} = 400 nm). Parallel to the surface (x direction) the source profiles are homogeneous. Therefore, 1 nm is sufficient to take the influence of the anisotropic transport into account. Due to numerical issues the sample thickness is limited to 400 nm. Nevertheless, the surface flux from the back surface is much lower than at the front, thus limiting the influence of the restricted sample size in the calculation.

Full CRDS simulations for implantation of D, relaxation and desorption of D, including the surface fluxes of MV and SIA, into the two Be single crystal orientations are shown in Fig. 2. During the implantation phase (from $t = t_0$ to t_i), the temperature T is held constant at 300 K and the source terms S introduce H, MV and SIA into the sample. The source profiles are taken from static SDTrim.SP calculations [4], using deuterium as a projectile. If the implantation energy is varied, the source profiles change accordingly. During this phase, all reactions (equ. 3-6) are active, so the Frenkel pairs annihilate, diffuse or trap hydrogen. This approach overestimates the number of introduced Frenkel pairs, because in reality most point defects heal already during the cascade on a time scale of picoseconds. However, the evolution of the defects on the time scale of diffusion is followed explicitly. The trapped hydrogen inventory and depth profiles for all species are therefore calculated only based on the source terms given by SDTrim.SP. The energy barriers are taken from DFT calculations [1] and summarized in Tab. 1. Note that only the frequency factor of the de-trapping reaction 4 had to be adjusted from 10^{13} (conservative choice) to 5×10^{10} s^{-1} in order to quantitatively reproduce all the experimental data presented here. The simulations are insensitive to the choice of the diffusion barrier of H_2, as long as it is between 0.2 and 0.4 eV and is isotropic. It

is therefore in the range of DFT [1] and other experimental values [5]. The hydrogen-vacancy complexes HV are assumed to be immobile.

If the diffusivities D_x and D_z are chosen such that the basal planes are perpendicular to the surface (i.e. Be(11-20), the migration of SIA towards the surface is fast), a H retention factor R (equ. 12) of ~1 is calculated at the end of the implantation ($t=t_i$). This is due to the fast annihilation of the SIA at the surface, while the MV remain in the sample to trap H.

$$R = \left(\int_{z=z_0}^{z_{max}} \rho_{HV}(t_i) + \rho_H(t_i) dz \right) \left(\int_{t=t_0}^{t_i} \int_{z=z_0}^{z_{max}} S dz dt \right)^{-1} \quad [12]$$

If the diffusion is slow towards the surface (Be(0001), basal planes are parallel to the surface), then locally the annihilation reaction (equ. 6) dominates, thus decreasing the density of MV available for trapping of H. This mechanism can quantitatively explain the reduction of the retention factor to ~0.6 for the Be(0001) single crystal. This is shown in Fig. 1 where the reduced TPD peak area after the 3 keV implantation into Be(0001) as compared to Be(11-20) is quantitatively reproduced.

After the implantation phase, the sample is allowed to relax (t_i *to* t_R), where in the case of Be(11-20) the remaining MV diffuse to the surface. In the last phase of the calculation, the uniform sample temperature *T(t)* is ramped up according to the experimental procedure. Already at slightly elevated temperatures, all the remaining MV diffuse out of the sample, whereas the HV profile remains in the sample. This is the reason why the relaxation time of the sample can be quite short, as the sample will reach its steady state at the beginning of the

temperature ramp anyway. With increasing temperature, H starts to de-trap (equ. 4), while in parallel self-trapping, re-trapping, and diffusion of H, MV and SIA lead to a migration of all species through the sample. Eventually, all species reach the surface in a single peak, which temperature depends on the crystal orientation and implantation energy. The results of the simulations are in good agreement to the experimentally observed TPD peaks (Fig. 1).

One may expect that the behaviour of a polycrystal with randomly oriented crystallites would be a mixture between the two single crystal orientations, thus showing a TPD peak between 750 K and 770 K at 3 keV implantation energy and a temperature ramp of 0.7 K/s. However, the measured peak is much lower at 710 K. This indicates an enhanced migration path present in the polycrystal, presumably in the form of grain boundaries [6]. One possibility to implement this effect into the simulation is to deactivate the re-trapping and self-trapping reactions (equ. 3 and 5) during the temperature ramp phase. This leads automatically to the observed TPD peak at 710 K. The shoulder at around 760 K can therefore be interpreted as hydrogen desorption from crystallites that are large enough that H is re-trapped during the diffusion step towards the sample surface without taking the short-cut via grain boundaries. To test this mechanism, TPD spectra from polycrystals with different grain sizes are needed. The peak structures at lower temperature cannot be interpreted at the moment, but might be associated to trapping of multiple H trapped in a single vacancy.

To further test if the simulation reproduces the correct effective diffusivity (which is sensitive to the slope of the ramp), the temperature ramps are varied both experimentally and in the respective CRDS calculations. As shown in Fig. 3, the shift and shape of the TPD peaks is reproduced by the simulations for ramps from 0.1 to 2 K/s.

Note that equ. 1 with all reactions and diffusivities is unchanged during implantation, relaxation and temperature ramp, thus the proposed reactions are sufficient to explain the complete recycling behaviour of H in pure Be at low fluences. However, if the fluence is

increased (> 10^{21} m^{-2}), additional effects such as super-saturation and the formation of hydrides [7] occur. Additionally, it cannot be excluded that with increasing H flux, additional effects influence the H recycling (e.g. by increasing diffusivities). These effects will be addressed in future studies.

4. Summary:

We propose a model that can reproduce the recycling behaviour of hydrogen in Be at low fluxes and fluences in single and polycrystalline Be. It is based on energy barriers calculated by DFT and assumes an anisotropic transport of SIA with respect to the Be basal plane, and trapping and de-trapping reactions for hydrogen. As primary trap sites for hydrogen, monovacancies are suggested. The dynamics of implantation and retention are also implemented based on volumetric source rates given by SDTrim.SP calculations. The model assumes a self-trapping reaction, where a hydrogen atom in a solute (interstitial) position can displace a Be atom from its lattice position near another hydrogen-vacancy complex, thus creating a second hydrogen-vacancy complex and a free Be self-interstitial. There are indications by DFT that support this mechanism, because Be can be easily displaced if the lattice is already disturbed.

H retention in Be(0001) is reduced to ~ 60% in comparison to Be(11-20) with ~100% at low fluences. We attribute this to a smaller amount of available MV trap sites in the Be(0001). In Be(11-20) SIA diffusion to the surface (and annihilation there) is faster, leading to higher amount of remaining MV trap sites after D implantation.

D desorption temperatures are smaller in polycrystalline Be than in single crystalline Be. Modelling shows that the reduced desorption temperatures occur if the re-trapping process for single crystals is removed from the calculations. This is representing a greatly enhanced effective transport along grain boundaries. D diffusion in Be grains seems to be fast enough that no re-trapping occurs until D reaches a grain boundary, from which diffusion to the surface and desorption take place. However, small shoulders at higher temperatures in the release peaks indicate an additional contribution from single crystal-like desorption behaviour in large grains.

Captions:

Fig. 1: TPD spectra and 2D-CRDS simulations after implantation of D at 1 keV/D and 3 keV/D in Be(0001) and Be(11-20). D implantation fluences are 3×10^{19} m^{-2}.

Fig. 2: Surface fluxes of MVs, SIAs and H during 2D-CRDS simulations for Be(0001) and Be(11-20). Implantation of D occurs from t_0 to t_i. Relaxation of the system occurs between t_i and t_R. A heating ramp of 0.7 K/s is applied between t_R and t_{max}.

Fig. 3:

TPD spectra and 2D-CRDS simulations of D_2 desorption from polycrystalline Be at different heating ramps. D implantation parameters are 3 keV/D and fluences ~3×10^{19} m^{-2}. No selftrapping/ trapping during heating in the simulations.

Tab. 1:

Summary of diffusivities and frequency factors v for all species used in the CRDS modelling. Activation barriers used for the modelling are in very good agreement with DFT calculations.

*: Discrepancy between CRDS simulation and DFT calculation by Allouche [1].

**: Changed to fit to experimental data.

Fig 1:

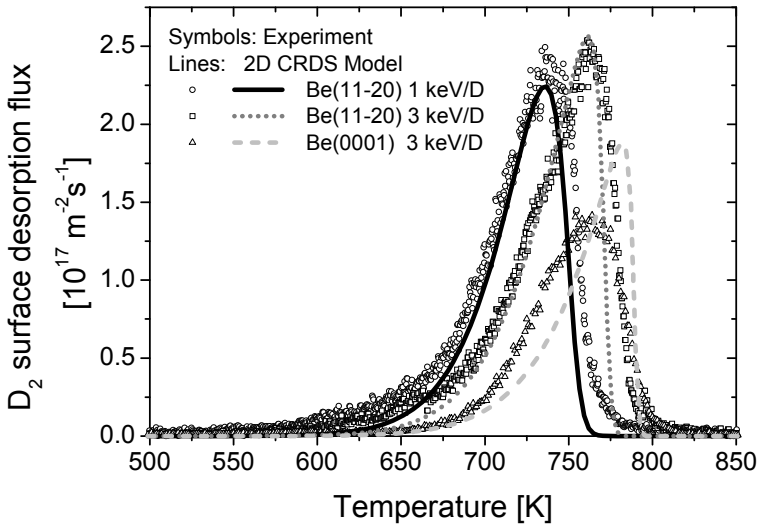
Symbols: Experiment
Lines: 2D CRDS Model
Be(11-20) 1 keV/D
Be(11-20) 3 keV/D
Be(0001) 3 keV/D
D2 surface desorption flux
[10^17 m^-2 s^-1]
Temperature [K]
0.0
0.5
1.0
1.5
2.0
2.5
500
550
600
650
700
750
800
850

Fig 2:

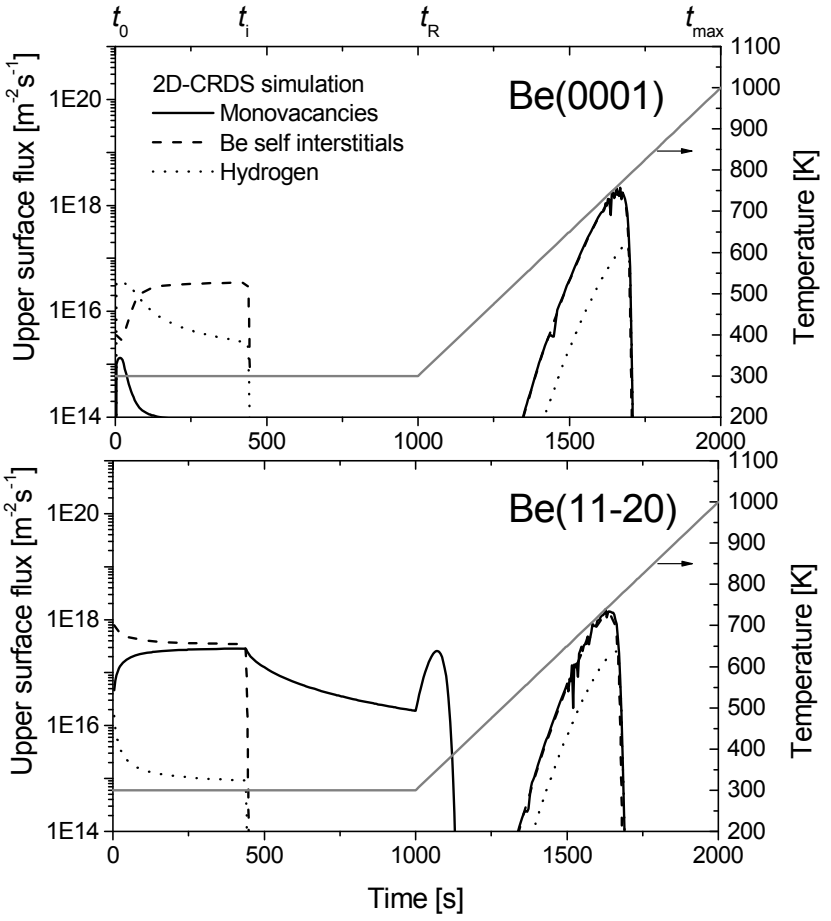
t_0
t_i
t_R
t_{max}
2D-CRDS simulation
Monovacancies
Be self interstitials
Hydrogen
Be(0001)
Be(11-20)
Upper surface flux [m^{-2}s^{-1}]
Temperature [K]
Time [s]
1E14
1E16
1E18
1E20
0
500
1000
1500
2000
200
300
400
500
600
700
800
900
1000
1100

Fig 3:

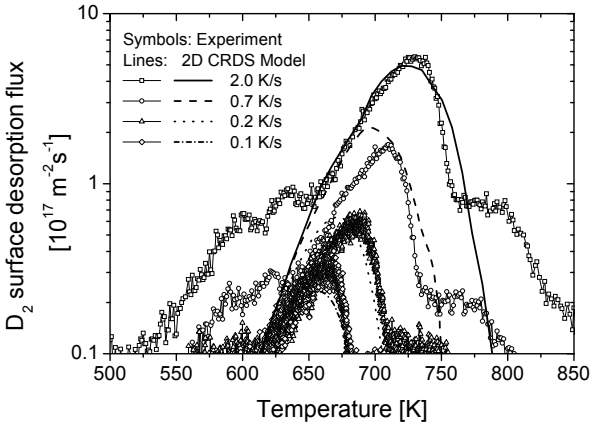
Symbols: Experiment
Lines: 2D CRDS Model
2.0 K/s
0.7 K/s
0.2 K/s
0.1 K/s
D2 surface desorption flux
[10^17 m^-2 s^-1]
Temperature [K]
10
1
0.1
500
550
600
650
700
750
800
850

Tab. 1:

		CRDS: D_0, ν	CRDS: ΔE [eV]	DFT: ΔE [eV]
Diffusion || to basal plane	H	3.11E-06	0.4 *	0.2 *
	MV	3.11E-06	0.7	0.7
	SIA	3.11E-06	0.4	0.4
Diffusion ⊥ to basal plane	H	7.68E-06	0.4	0.4
	MV	7.68E-06	0.7	0.7
	SIA	7.68E-06	0.004	0.004
Trapping	equ. 3	1.00E+13	0.4	0.4
De-trapping	equ. 4	5.00E+10 **	1.7	1.7
Self-trapping	equ. 5	1.00E+13	0.4	0.4
Annihilation	equ. 6	1.00E+13	0.004	0.004

References:

[1] A. Allouche, M. Oberkofler, M. Reinelt, and Ch. Linsmeier, J. Phys. Chem. C. 114 (2010) 3588
[2] Ch. Linsmeier, P. Goldstraß, and K.U. Klages, Phys. Scr. T94 (2001) 28
[3] M. Oberkofler and Ch. Linsmeier, Nucl. Fusion 50 (2010) 125001
[4] M. Oberkofler, M. Reinelt, and Ch. Linsmeier, Nucl. Instrum. Meth. B 269 (2011) 1266
[5] E. Abramov, M. Riehm, D. Thompson, and W. Smeltzer, J. Nucl. Mater. 175 (1990) 90
[6] U. von Toussaint, S. Gori, *Diffusion in polycrystalline Beryllium: An energy-landscape based approach using MD and TST*, to be submitted to J. Nucl. Mater.
[7] M. Reinelt and Ch. Linsmeier, J. Nucl. Mater. 390-391 (2009) 568